CO Oxidation on Gold-supported Iron Oxides: New Insights into Strong Oxide-Metal Interactions

Liang Yu[1,2], Yun Liu[1], Fan Yang[1,2], Jaime Evans,[3] José A. Rodriguez[4], Ping Liu[4]**

[1] Collaborative Innovation Center of Chemistry for Energy Materials, Xiamen University, Xiamen 361006, China

[2] State Key Laboratory of Catalysis, Dalian Institute of Chemical Physics, Dalian 116023, China

[3] Facultad de Ciencias, Universidad Central de Venezuela, Apartado 20513, Caracas 1020-A, Venezuela

[4] Chemistry Department, Brookhaven National Laboratory, Upton, NY 11973, USA

ABSTRACT

Very active FeO_x-Au catalysts for CO oxidation are obtained after depositing nanoparticles of FeO, Fe_3O_4 and Fe_2O_3 on a Au(111) substrate. Neither FeO nor Fe_2O_3 are stable under reaction conditions. Under an environment of CO/O_2, they undergo oxidation (FeO) or reduction (Fe_2O_3) to yield nanoparticles of Fe_3O_4 that are not formed in a bulk phase. Using a combined experimental and theoretical approach, we show a strong oxide-metal interaction (SOMI) between Fe_3O_4 nanostructures and Au(111), which gives the oxide special properties, allows the formation of an active phase and provides a unique interface to facilitate a catalytic reaction. Our work highlights the important role that the SOMI can play in enhancing the catalytic performance of the oxide component in metal-oxide catalysts.

1. INTRODUCTION

The strong metal-support interaction (SMSI) has been found to play essential roles in catalytic processes on metal-oxide catalysts.[1-3] The term was used in 1978 by Tauster to explain the negative effect in uptake properties of precious metals supported on titanium oxide.[1, 2] In contrast, promotion of the intrinsic activity and selectivity has been observed during many catalytic processes, e.g. water-gas shift, CO oxidation and ethanol oxidation, when using oxides as support to precious metals.[4-9] The special synergy between metals and oxide supports, often attributed to SMSIs, can reflect large electronic perturbations in the metals.[3, 10] In more broad terms, the SMSI can introduce special sites at the metal-oxide interface[7, 9, 11-14] and induce the structural variation on the metal particles,[15, 16] which directly affect the bonding strength of an adsorbate and therefore the catalytic performances.

In previous studies examining the SMSI in metal-oxide catalysts, the emphasis has been on variations in the chemical and catalytic properties of the metal component.[1-3] Studies of surface science have revealed that at a metal-oxide interface the metal can alter the electronic and chemical properties of the oxide,[15-17] and in some cases, to confine the under-saturated active sites at the interface. In principle, one could take advantage of such a phenomenon in the rational design of efficient catalysts. The present study reports a type of strong oxide-metal interaction (SOMI) that leads to a high catalytic activity. It enables an important phase transition in the oxide component under reaction conditions. Such transition leads to the formation of an active phase, which is not stable in bulk and provides a unique interface to facilitate the catalytic reaction. The CO oxidation on a Au(111)-supported iron oxide (FeO_x) model catalyst is presented here as a case study. FeO_x-supported Au nanoparticles have been found as one of the most active catalysts for CO oxidation.[17-23] Several active sites were proposed involving metallic

Au sites,[24] interfacial Au ions[21] or the combination of the two Au species.[22, 23] Little attention has been paid to the optimization of the oxide phase in the catalyst or to details of the reaction mechanism. Only recently, a Mars–van–Krevelen (MvK) mechanism was hypothesized at the interface,[25] where FeO_x provided lattice oxygen to react with CO adsorbed onto neighboring Au and produce CO_2 together by the reduction of Fe^{3+} to Fe^{2+}.[18] In addition, the roles that FeO_x can play in the powder Au/FeO_x catalysts still remain unknown.

To gain better understanding of the reaction mechanism and active phase, we carried out a combined scanning tunneling microscopy (STM), X-ray photoemission spectroscopy (XPS) and density functional theory (DFT) study to investigate CO oxidation on inverse catalysts for Au/FeO_x: FeO_x nanostructures deposited on Au(111). A previous work using a Fe_2O_3/Au(111) model catalyst identified the interface as the active region, though the phase variation of Fe_2O_3 during the reaction was not studied.[26] FeO_x can adopt different phases (Figure S1) depending on the CO : O_2 ratio. It is known that FeO/Pt(111) is more active than pure metal surfaces for CO oxidation.[14, 27] Thus, we investigated the catalytic performance of FeO/Au(111), Fe_3O_4/Au(111) and Fe_2O_3/Au(111). Each one of these systems has well-defined features in STM and XPS.[28-31] Our results showed that FeO/Au(111) and Fe_2O_3/Au(111) underwent significant phase transition under typical CO oxidation conditions. As we will see below, the SOMI promoted the stability of a Fe_3O_4(111) thin film and the perimeter sites between Fe_3O_4(111) and Au(111) were identified as the active sites to catalyze CO oxidation among various phases formed during CO oxidation. The present study highlights the essential roles that the SOMI can play in promoting the catalysis on metal-oxide systems.

2. EXPERIMENTAL SECTION

2.1 Surface science studies. The microscopy studies were performed in a customized Createc LT-STM chamber (base pressure < 6×10^{-11} mbar). The Au(111) single crystal was cleaned by cycles of Ar^+ sputtering (1.2 keV, 10 μA) at 300K, followed by annealing at 800 K for 10min. FeO nanolayers were deposited onto the Au(111) surface by evaporating Fe atoms in 1.3×10^{-7} mbar O_2 at 300 K, then annealed to 600 K. Fe_3O_4 was prepared by oxidize FeO/Au(111) in 1.3×10^{-6} mbar O_2 at 500 K for 10 min. Fe_2O_3 were deposited following the reported procedure.[30] Fe was first deposited on the clean Au(111) at 300K, then oxidized in 3×10^{-8} mbar NO_2 for 30 min at 500 K, followed by annealing at 600K. Fe_3O_4 was prepared by further annealing Fe_2O_3 on Au(111) to 700K in UHV.[28]

Additional characterization studies were carried out in a system which combines a batch reactor and a UHV chamber.[4, 9] The UHV chamber (base pressure ~ 1 x 10^{-10} Torr) was equipped with instrumentation for XPS, low-energy electron diffraction, ion-scattering spectroscopy (ISS), and thermal-desorption mass spectroscopy. XPS and Auger spectra were acquired using Mg Kα radiation. The FeO_x/Au(111) surfaces were prepared as described in refs [26, 28, 30]. The area of the gold surface covered by iron oxide was estimated using STM images or a combination of ISS and XPS. The FeO_x/Au(111) sample could be transferred between the UHV chamber and reactor without exposure to air. Typically, it was transferred to the batch reactor at ~ 298 K, the reactant gases were introduced (5 Torr of CO and 5 Torr of O_2), and then the sample was rapidly heated to the reaction temperature (575 K). Product yields were analyzed by a gas chromatograph.[4, 26] The amount of molecules produced was normalized by the active area exposed by the sample. Carbon deposition reduces the catalytic activity of the FeO_x/Au(111) surfaces over time.[26] In our study, we focused on the initial rate for CO oxidation which is a very useful parameter when investigating the performance of a catalyst.[26]

2.2 DFT calculations. Periodic DFT calculations were performed using the Vienna Ab-initio Simulation Package (VASP).[32-36] The projector augmented-wave pseudopotentials and a cutoff energy of 400 eV for the plane-wave basis set were adopted.[32, 37] The generalized gradient approximation (GGA) method with Perdew-Burke-Ernzerhof (PBE) functionals for the exchange-correlation term was used.[38, 39] The Monkhorst-Pack scheme was used for sampling the Brillouin zone.[40] The Au(111) slab model for supporting the FeO_x was built using three layers of atom with the bottom two layers fixed during structural relaxations. The top layer of Au(111) and all Fe and O were fully relaxed. The vacuum thickness of all models were set as ~10Å. Spin polarization was considered throughout the calculations. To correctly describe the strongly correlated iron oxides, the DFT+U approach was used, as implemented by Dudarev,[41] with U_{Fe}-J_{Fe}=3eV. The transition states were searched using the improved dimer method.[42, 43]

3. RESULTS and DISCUSSION

3.1 Structures. To determine the phase diagram of FeO_x/Au(111), various structures were studied using STM, XPS and DFT. Upon exposure to oxygen, STM observed a phase transformation from FeO/Au(111) (Figure 1a) to Fe_3O_4/Au(111) (Figure 1b) and Fe_2O_3/Au(111) (Figure 1c), which all agreed well with previous studies.[28-31] FeO is a Fe-O bilayer, which grows epitaxially on the Au(111) support and exposes the FeO(111) surface. Under oxidative conditions, the lattice of FeO_x remains with a hexagonal (111)-like periodicity; however, the height varies from monolayer FeO(111) to multilayer Fe_3O_4(111) and Fe_2O_3(001) structures. As shown in Figure 2, the supported islands of FeO, Fe_2O_3 and Fe_3O_4 exhibit distinct Fe $2p_{3/2}$ binding energies in XPS.[28-31]

3.2 Catalytic activity and stability of the FeO_x/Au(111) systems. A previous study of CO oxidation on Fe_2O_3/Au(111)[26] revealed that a maximum of catalytic activity occurs when the surface is covered with ~ 0.4 ML of the iron oxide. Accordingly in this work, we investigated the catalytic activity of surfaces generated by depositing 0.4 ML of FeO, Fe_3O_4 and Fe_2O_3 on a Au(111) substrate. Figure 2 shows Fe $2p_{3/2}$ XPS spectra acquired before and after exposure of the surfaces to the reactants.

Exposure of FeO/Au(111) to the reactants for CO oxidation induces the transformation of FeO into Fe_3O_4 and some carbon-containing species (FeC_x) as confirmed by XPS studies (Figure 2a).[28, 30, 44] On the other hand, the oxide overlayer in Fe_2O_3/Au(111) is also not stable under reactions conditions and transforms into Fe_3O_4 and FeC_x as well (Figure 2a).[28,31,44,45] In contrast, Fe_3O_4 is the only oxide layer on Au(111), being able to survive during CO oxidation, though the formation of FeC_x cannot be avoided (Figure 2b). Thus, the results of XPS indicate that the active phase in these systems is Fe_3O_4 supported on Au(111).

We compared the catalytic activity of the different iron oxide/gold systems. Figure 3 displays the initial reaction rates for CO oxidation on FeO/Au(111), Fe_3O_4/Au(111) and Fe_2O_3/Au(111). A previous study showed that initial reaction rates were quite useful to study the intrinsic activity of a Fe_2O_3/Au(111) surface before variations in activity due to a change in the oxidation state of iron or carbon deposition.[26] In essence, we are comparing in Figure 3 the activity of systems that initially have the iron in oxidation states of +2 (FeO), +3 (Fe_2O_3) or both (Fe_3O_4). It is clear that the more active catalysts are those that contain a significant concentration of Fe^{2+}.

Unfortunately, FeO/Au(111) is too active and part of it eventually transforms into Fe_3O_4/Au(111) (Figure 2). More importantly, FeO/Au(111) is deactivated by deposition of FeC_x

on the surface. An analysis of the corresponding C 1s XPS spectra, Figure 4, pointed to the deposition of C[44,45] and the formation of carbonates on the surface of the catalysts.[45] The accumulation of surface FeC_x species increased in the sequence: Fe_2O_3 < Fe_3O_4 << FeO (Figure 5). The large accumulation of carbon-containing species on FeO/Au(111) is a serious problem that eventually in the long term kills the catalytic activity in the catalyst. In this respect, Fe_3O_4/Au(111) seems a better choice as a catalyst. It has stable and enough Fe^{2+} sites to yield very good catalytic activity and does not get completely poisoned by carbon or carbonate species. On the Fe_3O_4/Au(111) catalyst, the rate of CO oxidation decreased from an initial value of 14×10^{15} molecules cm^{-2} s^{-1} to a value of 11×10^{15} molecules cm^{-2} s^{-1} after 60 minutes of reaction.

3.3 Phase diagram under CO oxidation conditions: DFT studies. The XPS results in Figure 2a point to the low stability of FeO/Au(111) and Fe_2O_3/Au(111) under reaction conditions. DFT calculations were employed to investigate the stability of FeO_x layers in different oxidation states. As shown in Figure 6, structures of FeO, Fe_3O_4, and Fe_2O_3 on the Au(111) surface were constructed based on the STM measurements (Figure 1). For FeO/Au(111) (Figure 6a), a FeO(111) bilayer supported on Au(111) was considered, which reproduced well the periodicity of the moiré pattern as reported.[31] According to our calculations, FeO(111) interacts with Au(111) via Fe and the FeO(111) overlayer is terminated by O. The average distance between O atoms is 3.05Å which is in the range of reported values of 3.0 ~ 3.3 Å (Figure 6a).[29, 31] For Fe_3O_4(111)/Au(111) (Figure 6b) and Fe_2O_3(001)/Au(111) (Figure 6c), the models were packed according to the corresponding oxide bulk and the lattice distance of between the top-layer O atoms matches that from STM measurements (Figure 1).[28, 30] In term of thickness, the multilayered Fe_3O_4(111) and Fe_2O_3(001) were set containing three layers of Fe with thicknesses

of ~6 Å (Figure 6b,c) according to the reported STM height measurements (5 ~ 7 Å, Figure 1).[28, 30] To keep the bulk Fe/O ratio and the thickness measured in STM, we tested different terminations at both interface and surface for Fe_3O_4(111) and Fe_2O_3(001) layers. The Fe-terminated interface and O-terminated surface turned out to be the most stable. In addition, after examining the XPS data in Figure 2, we also considered the possible reduction of FeO_x to Fe by CO, which could also enable the CO dissociation and therefore formation of FeC_x. To describe the nanoscale effect, both Fe and Fe_3C were simulated as nanoparticles (Figure S1). The possibility of aggregation of the nanostructures under the reaction conditions was also included by using FeO_x, Fe and Fe_3C bulk to describe the big island aggregated during the reaction (Figure S1).

Figure 7 shows the DFT-calculated phase diagram of FeO_x/Au(111) under exposures of CO and O_2 at 575 K (see supporting for the details). Two cases were studied. One is for FeO_x nanostructures (Figure 7a) and the other is for FeO_x bulk (Figure 7b). In both cases, Fe and Fe_3C in the form of NP and bulk were included. Our results show that under the conditions studied, Fe is not stable, being either oxidized to FeO_x or reduced to Fe_3C. Fe_3C in the phase of bulk or big particles is likely to form, while the NP conformations cannot survive (Figure 7). FeO_x/Au(111) undergoes significant phase transformation depending the reaction conditions (Figure 7a). Increasing the CO chemical potential or pressure leads to the reduction from Fe_2O_3/Au(111) to Fe_3O_4/Au(111), FeO/Au(111) and eventually the formation of Fe_3C, while the reverse transformation can occur on raising O_2 pressure. In the case of considering FeO_x bulk (Figure 7b), only Fe_2O_3 and Fe_3C exist and they can transform directly to each other under the reductive or oxidative conditions studied without being trapped in any intermediate phase. Such behavior is different from FeO/Pt(111). Depending on the conditions (CO:O_2 between 1:5 and 5:1, 400-

450K), with Pt(111) as the support the FeO overlayer either stays or transforms into $FeO_{x(1<x<2)}$, which is active to CO oxidation.[46]

More importantly, the calculated phase diagram tells us about the possible phases formed in the pressure range of CO and O_2 for CO oxidation, which is highlighted as the square in Figure 7. The unique SOMI between FeO_x and Au(111) allows a significant phase transformation under typical CO oxidation conditions. It ranges from Fe_3O_4(111) nanolayer supported Au(111) and Fe_2O_3 bulk all the way to Fe_3C. It seems to indicate that the catalysts in the form of bulk-like big particles are likely to be Fe_3C and Fe_2O_3, while those adopting nanostructures are mostly Fe_3O_4/Au(111). That is, the SOMI with Au(111) is able to selectively stabilize the Fe_3O_4 phase in the form of nanolayers, which cannot survive in bulk conformation, but, as it will be seen below, are very active under CO oxidation condition. The stable phases of FeO_x/Au(111) under CO oxidation conditions agreed well with our experimental observations (Figure 2). Features appear at ~ 709 eV that denote the formation of a small amount of Fe carbide (FeC_x).[18] This is consistent with the DFT calculations. Fe carbides are formed during the reaction on all three FeO_x/Au(111) surfaces (Figure 2) but the largest amount of carbon is seen on the FeO/Au(111) system (Figures 4 and 5).

3.4 Active phase towards CO oxidation: DFT studies. Now the question is which of the phases identified is active for CO oxidation. We employed DFT to investigate the CO oxidation on the surfaces of Fe_3C bulk, Fe_2O_3 bulk and Fe_3O_4/Au(111). For Fe_3C and Fe_2O_3, the most stable surfaces, i.e. Fe_3C(001) and Fe_2O_3(001),[28, 30] were considered. The results show that the Fe_3C(001) surface is highly active for adsorption and dissociation of O_2. As a result, thermodynamically the formation of oxygen overlayer on the surface (-2.23 eV, Figure S2a) is more favorable than the adsorption of CO (-1.0 eV). Accordingly, Fe_3C(001) surface tends to be

poisoned by the strongly adsorbed oxygen species, which blocks the CO oxidation and therefore CO oxidation. That is, Fe_3C is not active for CO oxidation. On the Fe_2O_3(001) surface, our calculated partial density of states (PDOS) show that the Fe cations are in +3 (Figure 8). The Fe^{3+} allows efficient generation of oxygen vacancies and the reduction of Fe^{3+} to Fe^{2+} by CO, which eventually leads to the formation of very stable hexadentate carbonate structure embedded into a six-membered ring of iron, as shown in Figure S2b. Decomposition of such carbonate to CO_2 is highly endothermic (2.12 eV), which is extremely difficult to occur. As a consequence, Fe_2O_3(001) is passivated by the carbonate species and should also not be an active phase for CO oxidation. Similar situation is also observed for the terrace or overlayer of Fe_3O_4(111) on Au(111), where Fe^{3+} is present in the surface layer according to the calculated PDOS (Figure 8). As a result, the interaction with CO also produces the carbonate species in the hexadentate structure (Figure S2c). Again, the decomposition of carbonate to CO_2 is highly inhibited (1.88 eV). Therefore, the Fe_3C bulk, Fe_2O_3 bulk and the terrace of a Fe_3O_4(111) overlayer on Au(111) are also not active for CO oxidation.

We now move to the Fe_3O_4/Au(111) interface. Due to the SOMI, only Fe_3O_4 nanostructures on Au(111) survives (Figure 7) and exposes the metal-oxide interfacial sites under CO oxidation, which have been identified as the active sites for FeO_x/Pt(111).[47] Here, we built a strip model of Fe_3O_4 on the basis of the Fe_3O_4(111) overlayer structure on Au(111) (Figure 6b) to simulate the interfaces. The structure contains two interfaces, i.e. Fe_3O_4(111)/Au(111) and Fe_3O_4(100)/Au(111), as shown in Figure S3. We calculated the formation energy of the Fe_3O_4(111) and Fe_3O_4(100) surfaces, which is -0.45 and -0.47 eV/Å^2 respectively. It indicates that the two surfaces have very close stability. Thus we considered both interfaces for the study of CO oxidation.

According to the DFT-optimized potential diagram (Figure 9a), at the interface of Fe_3O_4(111)/Au(111) CO oxidation undergoes the MvK mechanism as observed for FeO_2/Pt(111).[25] CO adsorbs on the interfacial Au sites (ii, $CO_{(ads)}$, Figure 9a), rather than the interfacial Fe^{3+} sites on the surface according to the PDOS (3, Figure 8). Again, Fe^{3+} at the interface promotes the $CO_{(ads)}$ to react firstly with a interfacial lattice oxygen, which likely hinders the overall reaction with an overall barrier of 1.20 eV. It is then followed by the barrierless desorption of the produced CO_2 and the generations of an oxygen vacancy and two reduced Fe ion sites (iv, Figure 9a), likely Fe^{2+} (3 next to the oxygen vacancy, Figure 8). Fe^{2+} behaves differently from Fe^{3+}, which does not favor the formation of oxygen vacancy, but is active to adsorb and dissociate O_2. In this case the barrier for direct O-O bond cleavage is 0.88 eV (v, Figure 9a), where the synergy between Au and Fe helps in stabilizing the dissociated O species ($O_{(ads)}$) and therefore lowering the barrier (vi, Figure 9a). Such hybrid site also allows another $CO_{(ads)}$ to attack one of the $O_{(ads)}$ and form CO_2 with a barrier of 1.22 eV (vii, Figure 9a). The left $O_{(ads)}$ fills the oxygen vacancy previously produced and restores Fe^{3+} (i, Figure 9a). Due to the missing participation of Au in binding, carbonate is unstable in this case, displaying highly activated formation (barrier, 2.19 eV, Figure S4a).

At the interface of Fe_3O_4(100)/Au(111), CO oxidation follows Langmuir-Hinshelwood (LH) mechanism. The Fe ions that directly interact with Au(111) (2, Figure 8) and sit at the edge of the middle Fe_3O_4(100) layer (1, Figure 8) display similar electronic structure as the interfacial Fe^{2+} at Fe_3O_4(111)/Au(111). As a result, O_2 is adsorbed by bridging the two Fe sites (ii, Figure 9b). The sequential O-O bond cleavage is the most activated step along the LH pathway and has to overcome a barrier of 1.73 eV, which is higher than that at the Fe_3O_4(100)/Au(111) interface (1.20 eV). An additional $CO_{(ads)}$ at the interface removes the left $O_{(ads)}$ easily with a barrier of

1.18 eV (vi, Figure 9b). Although carbonate formation is highly activated at Fe_3O_4(100)/Au(111) (barrier, 1.35 eV, Figure S4b) is less activated than Fe_3O_4(111)/Au(111), the carbonate decomposition on both interfaces is faster than the formation. Therefore, both interfaces behave differently from the bulk surfaces of Fe_3O_4 and Fe_2O_3, being able to hinder the carbonate poisoning, but still facilitating CO oxidation; yet Fe_3O_4(111)/Au(111) interface is likely more active than Fe_3O_4(100)/Au(111) towards CO oxidation, where the maximum barrier for all the elementary steps is ~1.20 eV and the reaction should proceed well at 575K. Indeed, a high CO oxidation activity on Fe_3O_4/Au(111) was observed experimentally (Figure 3). In agreement with the DFT calculations, Fe^{2+} sites were found to be active and led to bigger activity for CO oxidation.

4. SUMMARY AND CONCLUSION

Our combined theory-experiment study reported a significant phase transition of FeO_x/Au(111) during CO oxidation. Fe_3C, Fe_2O_3 and Fe_3O_4/Au(111) were the three phases which can coexist under the reaction conditions, while Fe_3O_4/Au(111) was identified as the only active phase to catalyze CO oxidation. The SOMI plays an essential role in promoting the CO oxidation on FeO_x/Au(111) in various ways. The SOMI enables the stabilization of Fe_3O_4 nanostructures under reaction condition, while Fe_3O_4 cannot survive even in bulk conformation. In addition, the SOMI is able to tune the catalytic properties at the Fe_3O_4/Au(111) interface, being able to catalyze CO oxidation efficiently via the LH or MvK mechanism. It allows the facile generation of oxygen vacancies by CO and therefore active Fe^{2+}, which facilitates the O_2 dissociation. In addition, the binding of O-containing intermediates at the interface is moderate, strong enough to facilitate the O-O bond cleavage and weak enough to allow the facile removal of O by CO and prevent the poisoning by carbonate. During this process, Au also participates in the reaction

directly. Au sites not only interact with CO, but also help in providing moderate bind to dissociated O_2.

A series of fundamental studies for the deposition of oxide films on metal surfaces has shown that a metal can perturb the electronic and chemical properties of an oxide.[14, 27, 48, 49] Our work highlights the important roles that the SOMI can play in enhancing the catalytic performance of the oxide component in metal-oxide catalysts. Thus, it opens new routes to obtain special catalytic properties by selecting the proper combination of elements in a metal-oxide interface.

ACKNOWLEDGMENT

Work carried at BNL was financed by the US DOE, Office of BES (Grant No. DE-SC0012704). Calculations were performed using computational resources at the Center for Functional Nanomaterials, a DOE user facility at Brookhaven National Laboratory, and at the National Energy Research Scientific Computing Center (NERSC), which is supported by the Office of Science of the U.S. DOE under Contract No. DE-AC02-05CH11231. INTEVEP and IDB financed the work done at the UCV. Work carried at DICP was financed by NSFC (Grant No. 21303195, 21473191) and MOST (Grant No. 2013CB933100). We appreciate the valuable discussions with Prof. X. H. Bao.

AUTHOR INFORMATION

Corresponding Author

* J. A. Rodriguez, rodrigez@bnl.gov

* P. Liu, pingliu3@bnl.gov

ASSOCIATED CONTENT

Supporting Information. Details of computation on phase diagram, the structures used in DFT calculations. This material is available free of charge via the Internet at http://pubs.acs.org.

REFERENCES

1. Tauster, S. J., Strong metal-support interactions. *Acc. Chem. Res.* **1987,** 20, (11), 389-394.
2. Tauster, S. J.; Fung, S. C.; Garten, R. L., Strong metal-support interactions. Group 8 noble metals supported on titanium dioxide. *J. Am. Chem. Soc.* **1978,** 100, (1), 170-175.
3. Solymosi, F., Comments on electronic effects in strong metal-support interactions on titania-deposited metal catalysts. *J. Catal.* **1985,** 94, (2), 581-585.
4. Bruix, A.; Rodriguez, J. A.; Ramírez, P. J.; Senanayake, S. D.; Evans, J.; Park, J. B.; Stacchiola, D.; Liu, P.; Hrbek, J.; Illas, F., A new type of strong metal–support interaction and the production of H_2 through the transformation of water on Pt/CeO_2(111) and Pt/CeOx/TiO_2(110) catalysts. *J. Am. Chem. Soc.* **2012,** 134, (21), 8968-8974.
5. Chen, M. S.; Goodman, D. W., The structure of catalytically active gold on titania. *Science* **2004,** 306, (5694), 252-255.
6. Kowal, A.; Li, M.; Shao, M.; Sasaki, K.; Vukmirovic, M. B.; Zhang, J.; Marinkovic, N. S.; Liu, P.; Frenkel, A. I.; Adzic, R. R., Ternary Pt/Rh/SnO_2 electrocatalysts for oxidizing ethanol to CO_2. *Nature Mater.* **2009,** 8, 325-330.
7. Green, I. X.; Tang, W.; Neurock, M.; Yates, J. T., Spectroscopic observation of dual catalytic sites during oxidation of CO on a Au/TiO_2 catalyst. *Science* **2011,** 333, (6043), 736-739.
8. Acerbi, N.; Tsang, S. C. E.; Jones, G.; Golunski, S.; Collier, P., Rationalization of interactions in precious metal/ceria catalysts using the d-band center model. *Angew. Chem. Int. Ed.* **2013,** 52, (30), 7737-7741.
9. Graciani, J.; Mudiyanselage, K.; Xu, F.; Baber, A. E.; Evans, J.; Senanayake, S. D.; Stacchiola, D. J.; Liu, P.; Hrbek, J.; Sanz, J. F.; et al., Highly active copper-ceria and copper-ceria-titania catalysts for methanol synthesis from CO2. *Science* **2014,** 345, (6196), 546-550.
10. Campbell, C. T., Catalyst-support interactions: electronic perturbations. *Nat. Chem.* **2012,** 4, (8), 597-598.
11. Saavedra, J.; Doan, H. A.; Pursell, C. J.; Grabow, L. C.; Chandler, B. D., The critical role of water at the gold-titania interface in catalytic CO oxidation. *Science* **2014,** 345, (6204), 1599-1602.
12. Fu, Q.; Yao, Y.; Guo, X.; Wei, M.; Ning, Y.; Liu, H.; Yang, F.; Liu, Z.; Bao, X., Reversible structural transformation of FeO_x nanostructures on Pt under cycling redox conditions and its effect on oxidation catalysis. *Phys. Chem. Chem. Phys.* **2013,** 15, (35), 14708-14.
13. Fu, Q.; Yang, F.; Bao, X., Interface-confined oxide nanostructures for catalytic Oxidation reactions. *Acc. Chem. Res.* **2013,** 46, (8), 1692-1701.
14. Fu, Q.; Li, W.-X.; Yao, Y.; Liu, H.; Su, H.-Y.; Ma, D.; Gu, X.-K.; Chen, L.; Wang, Z.; Zhang, H.; et al., Interface-confined ferrous centers for catalytic oxidation. *Science* **2010,** 328, (5982), 1141-1144.

15. Willinger, M. G.; Zhang, W.; Bondarchuk, O.; Shaikhutdinov, S.; Freund, H.-J.; Schlögl, R., A case of strong metal–support interactions: combining advanced microscopy and model systems to elucidate the atomic structure of interfaces. *Angew.Chem. Int. Ed.* **2014,** 53, (23), 5998-6001.
16. Liu, P., Understanding the behavior of TiO_2(110)-supported Pd_7 cluster: a density functional study. *J. Phys. Chem. C* **2012,** 116, (48), 25337-25343.
17. Kang, Y. J.; Ye, X. C.; Chen, J.; Qi, L.; Diaz, R. E.; Doan-Nguyen, V.; Xing, G. Z.; Kagan, C. R.; Li, J.; Gorte, R. J.; et al., Engineering catalytic contacts and thermal stability: gold/iron oxide binary nanocrystal superlattices for CO oxidation. *J. Am. Chem.Soc.* **2013,** 135, (4), 1499-1505.
18. Li, L.; Wang, A.; Qiao, B.; Lin, J.; Huang, Y.; Wang, X.; Zhang, T., Origin of the high activity of Au/FeO_x for low-temperature CO oxidation: Direct evidence for a redox mechanism. *J. Catal.* **2013,** 299, (0), 90-100.
19. Zhao, K. F.; Qiao, B. T.; Wang, J. H.; Zhang, Y. J.; Zhang, T., A highly active and sintering-resistant Au/FeO_x-hydroxyapatite catalyst for CO oxidation. *Chem. Commun.* **2011,** 47, (6), 1779-1781.
20. Wu, B.; Zhang, H.; Chen, C.; Lin, S.; Zheng, N., Interfacial activation of catalytically inert Au (6.7 nm)-Fe_3O_4 dumbbell nanoparticles for CO oxidation. *Nano. Res.* **2009,** 2, (12), 975-983.
21. Herzing, A. A.; Kiely, C. J.; Carley, A. F.; Landon, P.; Hutchings, G. J., Identification of active gold nanoclusters on iron oxide supports for CO oxidation. *Science* **2008,** 321, (5894), 1331-1335.
22. Haruta, M.; Yamada, N.; Kobayashi, T.; Iijima, S., Gold catalysts prepared by coprecipitation for low-temperature oxidation of hydrogen and of carbon monoxide. *J. Catal.* **1989,** 115, (2), 301-309.
23. Haruta, M.; Tsubota, S.; Kobayashi, T.; Kageyama, H.; Genet, M. J.; Delmon, B., Low-temperature oxidation of CO over gold supported on TiO_2, α-Fe_2O_3, and Co_3O_4. *J. Catal.* **1993,** 144, (1), 175-192.
24. Deng, W.; Carpenter, C.; Yi, N.; Flytzani-Stephanopoulos, M., Comparison of the activity of Au/CeO2 and Au/Fe2O3 catalysts for the CO oxidation and the water-gas shift reactions. *Top. Catal.* **2007,** 44, (1-2), 199-208.
25. Lewandowski, M.; Groot, I. M. N.; Shaikhutdinov, S.; Freund, H. J., Scanning tunneling microscopy evidence for the Mars-van Krevelen type mechanism of low temperature CO oxidation on an FeO(111) film on Pt(111). *Catal. Today* **2012,** 181, (1), 52-55.
26. Yan, T.; Redman, D. W.; Yu, W.-Y.; Flaherty, D. W.; Rodriguez, J. A.; Mullins, C. B., CO oxidation on inverse Fe_2O_3/Au(111) model catalysts. *J. Catal.* **2012,** 294, (0), 216-222.
27. Sun, Y.-N.; Giordano, L.; Goniakowski, J.; Lewandowski, M.; Qin, Z.-H.; Noguera, C.; Shaikhutdinov, S.; Pacchioni, G.; Freund, H.-J., The interplay between structure and CO oxidation catalysis on metal-supported ultrathin oxide films. *Angew. Chem.* **2010,** 122, (26), 4520-4523.
28. Deng, X.; Lee, J.; Matranga, C., Preparation and characterization of Fe_3O_4(111) nanoparticles and thin films on Au(111). *Surf. Sci.* **2010,** 604, (7–8), 627-632.
29. Deng, X.; Lee, J.; Wang, C.; Matranga, C.; Aksoy, F.; Liu, Z., In situ observation of water dissociation with lattice incorporation at FeO particle edges using scanning tunneling microscopy and X-ray photoelectron spectroscopy. *Langmuir* **2011,** 27, (6), 2146-2149.

30. Deng, X.; Matranga, C., Selective Growth of Fe_2O_3 nanoparticles and islands on Au(111). *J. Phys. Chem. C* **2009,** 113, (25), 11104-11109.
31. Khan, N. A.; Matranga, C., Nucleation and growth of Fe and FeO nanoparticles and films on Au(111). *Sur. Sci.* **2008,** 602, (4), 932-942.
32. Kresse, G.; Joubert, D., From ultrasoft pseudopotentials to the projector augmented-wave method. *Phys. Rev. B* **1999,** 59, (3), 1758-1775.
33. Kresse, G.; Hafner, J., Ab initio molecular dynamics for liquid metals. *Phys. Rev. B* **1993,** 47, (1), 558-561.
34. Kresse, G.; Hafner, J., Ab initio molecular-dynamics simulation of the liquid-metal–amorphous-semiconductor transition in germanium. *Phys. Rev. B* **1994,** 49, (20), 14251-14269.
35. Kresse, G.; Furthmuller, J., Efficiency of ab-initio total energy calculations for metals and semiconductors using a plane-wave basis set. *Comp. Mater. Sci.* **1996,** 6, (1), 15-50.
36. Kresse, G.; Furthmüller, J., Efficient iterative schemes for ab initio total-energy calculations using a plane-wave basis set. *Phys. Rev. B* **1996,** 54, (16), 11169-11186.
37. Blöchl, P. E., Projector augmented-wave method. *Phys. Rev. B* **1994,** 50, (24), 17953-17979.
38. Perdew, J. P.; Burke, K.; Ernzerhof, M., Generalized gradient spproximation made simple. *Phys. Rev. Lett.* **1996,** 77, (18), 3865-3868.
39. Perdew, J. P.; Burke, K.; Ernzerhof, M., Generalized gradient approximation made simple [Phys. Rev. Lett. 77, 3865 (1996)]. *Phy. Rev. Lett.* **1997,** 78, (7), 1396-1396.
40. Monkhorst, H. J.; Pack, J. D., Special points for Brillouin-zone integrations. *Phys. Rev. B* **1976,** 13, (12), 5188-5192.
41. Dudarev, S. L.; Botton, G. A.; Savrasov, S. Y.; Humphreys, C. J.; Sutton, A. P., Electron-energy-loss spectra and the structural stability of nickel oxide: an LSDA+U study. *Phys. Rev. B* **1998,** 57, (3), 1505-1509.
42. Henkelman, G.; Jónsson, H., A dimer method for finding saddle points on high dimensional potential surfaces using only first derivatives. *J. Chem. Phys.* **1999,** 111, (15), 7010-7022.
43. Heyden, A.; Bell, A. T.; Keil, F. J., Efficient methods for finding transition states in chemical reactions: Comparison of improved dimer method and partitioned rational function optimization method. *J. Chem. Phys.* **2005,** 123, (22), 224101.
44. Furlan, A.; Jansson, U.; Lu, J.; Hultman, L.; Magnuson, M., Structure and bonding in amorphous iron carbide thin films. *J. Phys.: Condens. Matter* **2015,** 27, (4), 045002.
45. de Smit, E.; van Schooneveld, M. M.; Cinquini, F.; Bluhm, H.; Sautet, P.; de Groot, F. M. F.; Weckhuysen, B. M., On the surface chemistry of iron oxides in reactive gas atmospheres. *Angew. Chem. Int. Ed.* **2011,** 50, (7), 1584-1588.
46. Sun, Y. N.; Qin, Z. H.; Lewandowski, M.; Carrasco, E.; Sterrer, M.; Shaikhutdinov, S.; Freund, H. J., Monolayer iron oxide film on platinum promotes low temperature CO oxidation. *J. Catal.* **2009,** 266, (2), 359-368.
47. Giordano, L.; Pacchioni, G.; Noguera, C.; Goniakowski, J., Identification of active sites in a realistic model of strong metal–support interaction catalysts: the case of platinum (1 1 1)-supported iron oxide film. *ChemCatChem* **2013**, 3867-3899.
48. Giordano, L.; Pacchioni, G., Oxide films at the nanoscale: new structures, new functions, and new materials. *Acc. Chem. Res.* **2011,** 44, (11), 1244-1252.
49. Pacchioni, G.; Freund, H., Electron transfer at oxide surfaces. The MgO paradigm: from defects to ultrathin films. *Chem. Rev.* **2013,** 113, (6), 4035-4072.

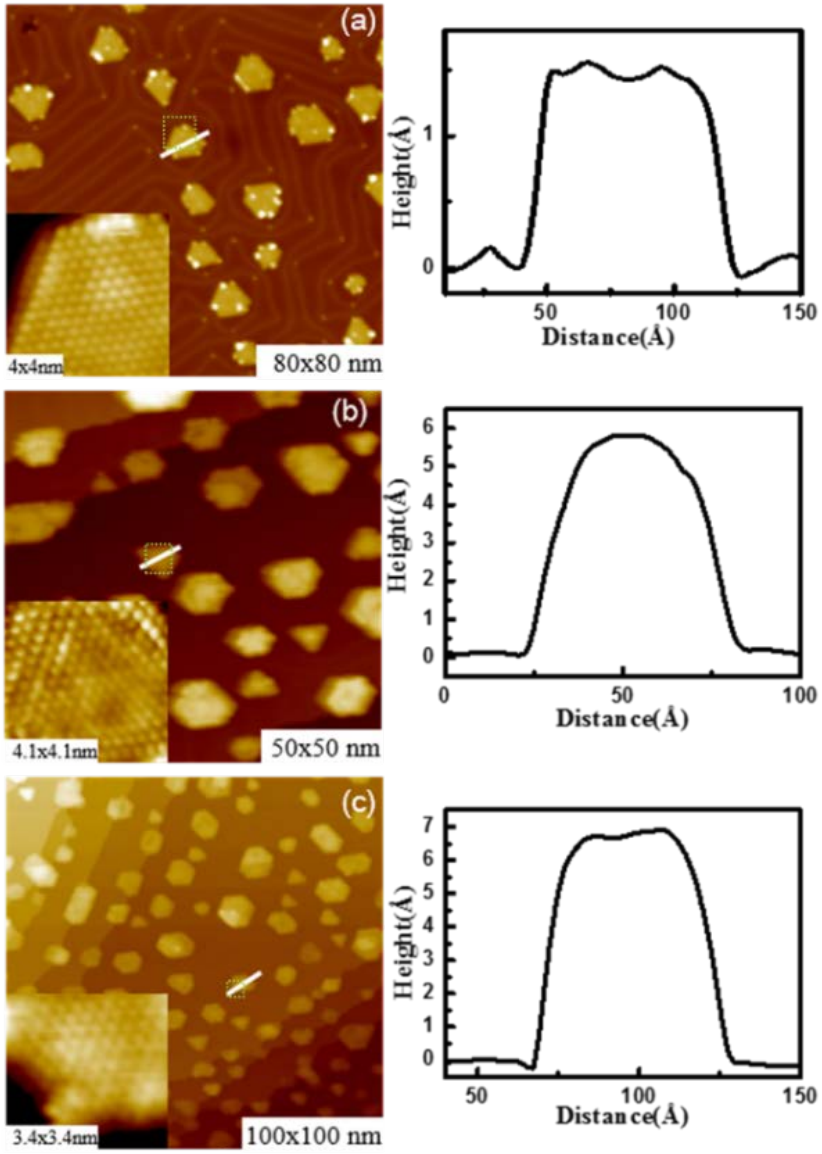

Figure 1. STM images of (a) FeO, (b) Fe3O4 and (c) Fe2O3 nanostructures on Au(111). The corresponding apparent heights of these nanostructures, as marked by white lines in STM images are plotted on the right side of the STM image, respectively. Inset of each STM image shows the atomic resolution of nanostructures. Scanning parameters for each inset image are: (a) Vs=0.05 V, It=2.0 nA; (b) Vs=0.5 V, It=3.0 nA; and (c) Vs=0.1 V, It=1.9 nA.

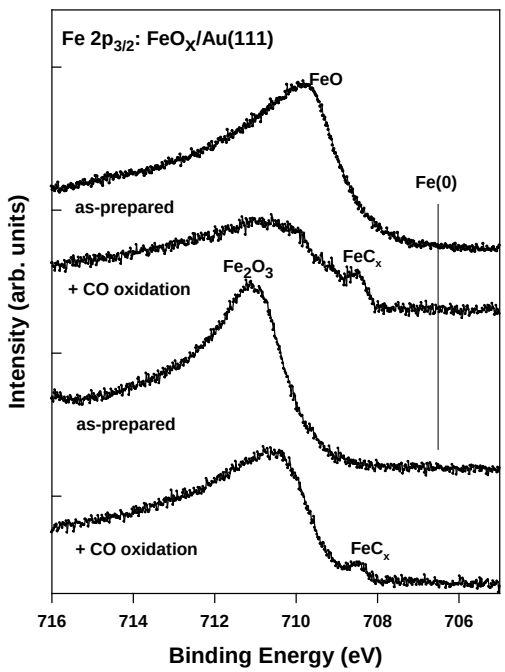

(a)

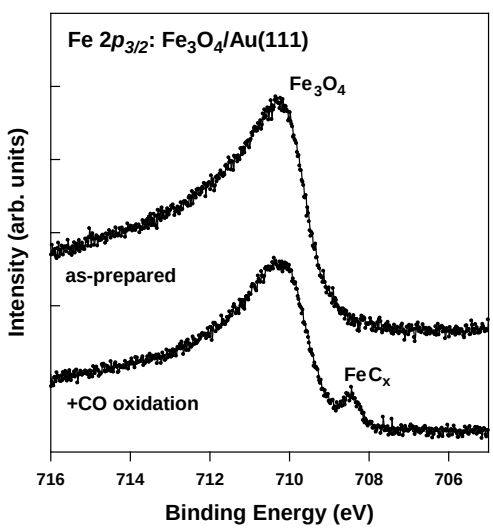

(b)

Figure 2. Fe $2p_{3/2}$ XPS spectra acquired before and after exposing FeO/Au(111) (a), Fe_2O_3/Au(111) (a) and Fe_3O_4/Au(111) (b) to a mixture of 5 Torr of CO and 5 Torr of O_2 for 5 minutes at 575 K. In the as-prepared surfaces, ~ 40% of the metal substrate was covered by FeO_x islands.

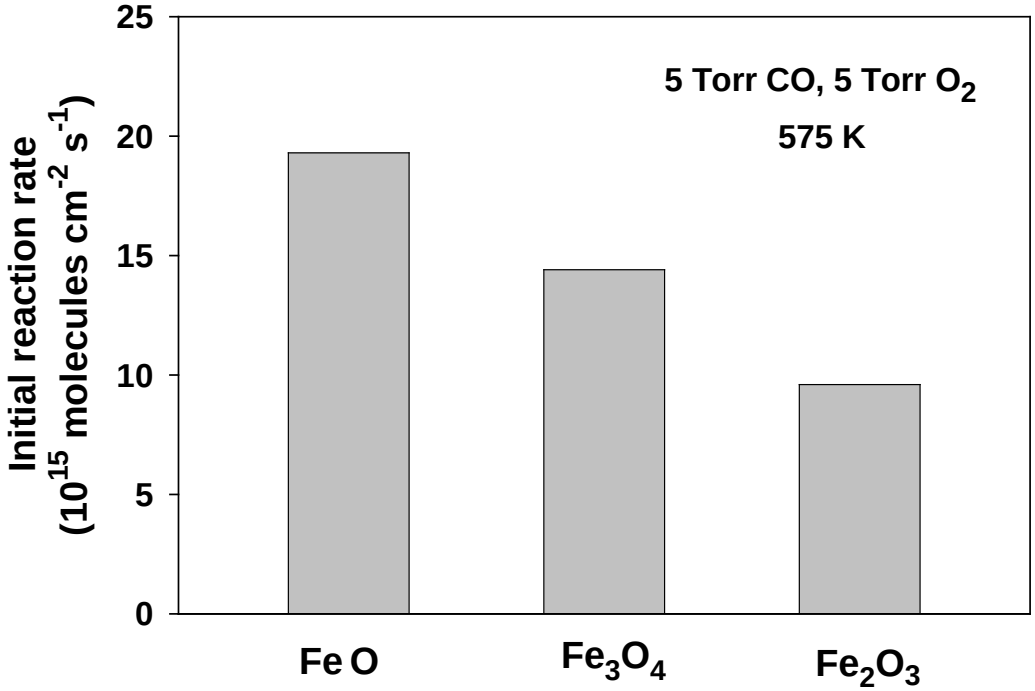

Figure 3. Initial reaction rate for the oxidation of CO into CO_2 on FeO/Au(111), Fe_3O_4/Au(111) and Fe_2O_3/Au(111) catalysts (5 Torr of CO and 5 Torr of O_2 at 575 K). No activity was seen for clean Au(111). In the as-prepared surfaces, ~ 40% of the metal substrate was covered by FeO_x islands.

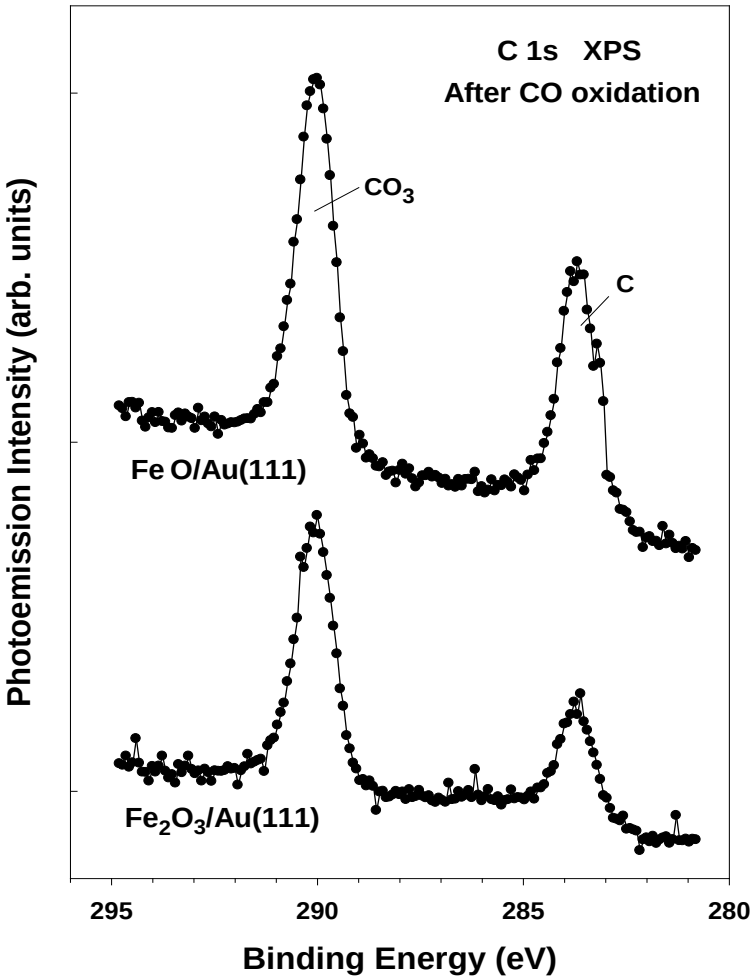

Figure 4**.** C 1s XPS spectra acquired after exposing FeO/Au(111) and Fe_2O_3/Au(111) to a mixture of 5 Torr of CO and 5 Torr of O_2 for 5 minutes at 575 K. In the as-prepared surfaces, ~ 40% of the metal substrate was covered by FeO_x islands.

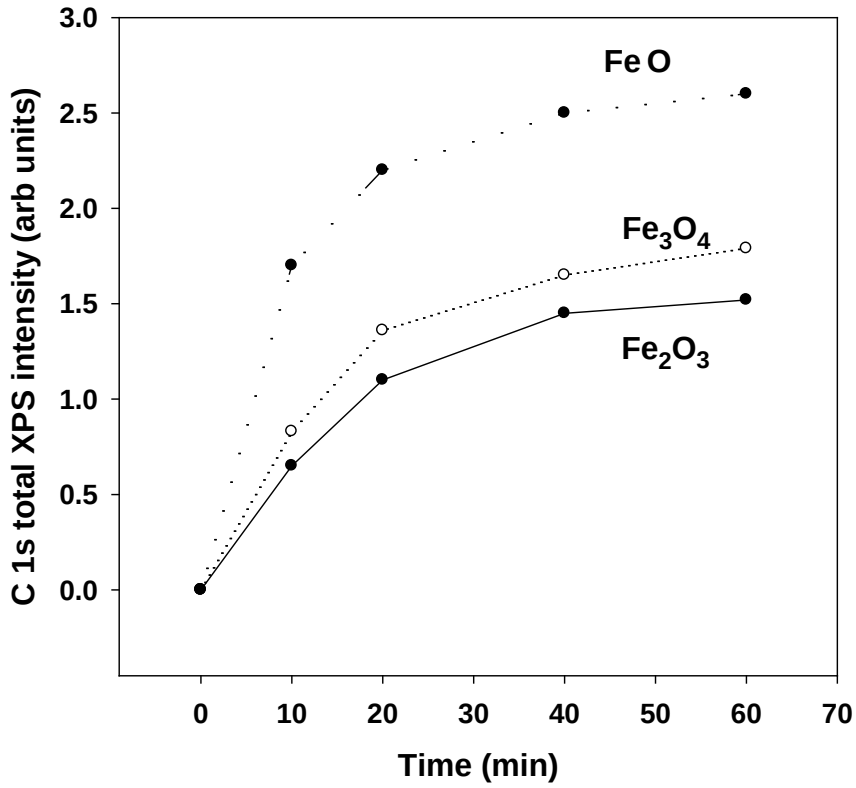

Figure 5. Accumulation of carbon-containing species on FeO/Au(111), Fe_3O_4/Au(111) and Fe_2O_3/Au(111) as a function of time upon exposure to a mixture of 5 Torr of CO and 5 Torr of O_2 at 575 K. In the as-prepared surfaces, ~ 40% of the metal substrate was covered by FeO_x islands.

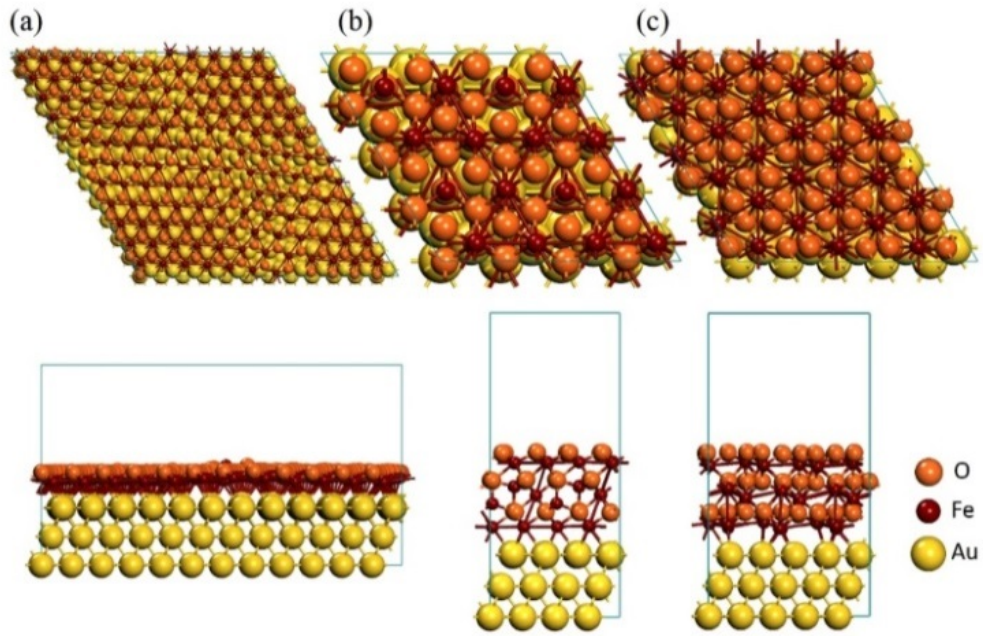

Figure 6. Supercells for modeling the overlayer structures of (a) FeO(111), (b) Fe_3O_4(111), and (c) Fe_2O_3(001) on Au(111) surface. The upper row is for top view and the bottom for side view.

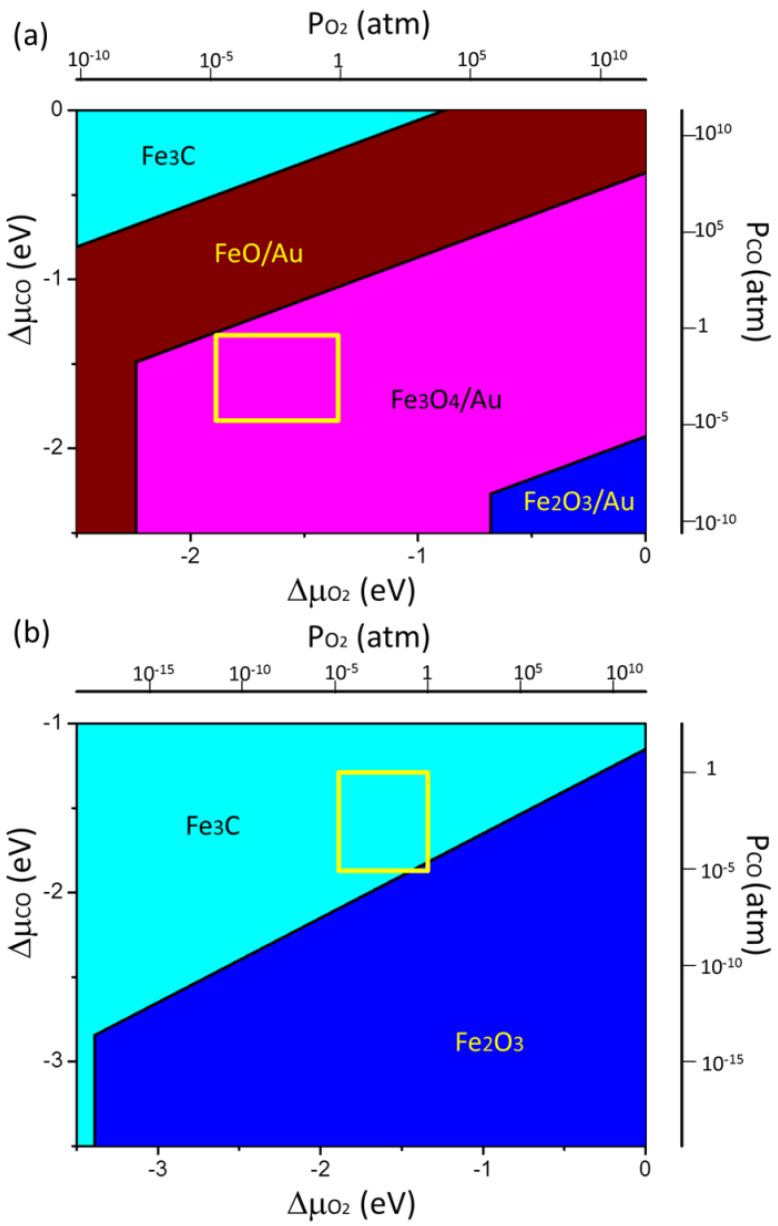

Figure 7**.** Phase diagram of iron species on Au(111) with morphology of (a) nanostructures and (b) bulk structures for FeO_x under the CO oxidation conditions at 575 K. The squares denote the pressure range of interest (10^{-5} ~1 atm) of CO and O_2 for CO oxidation.

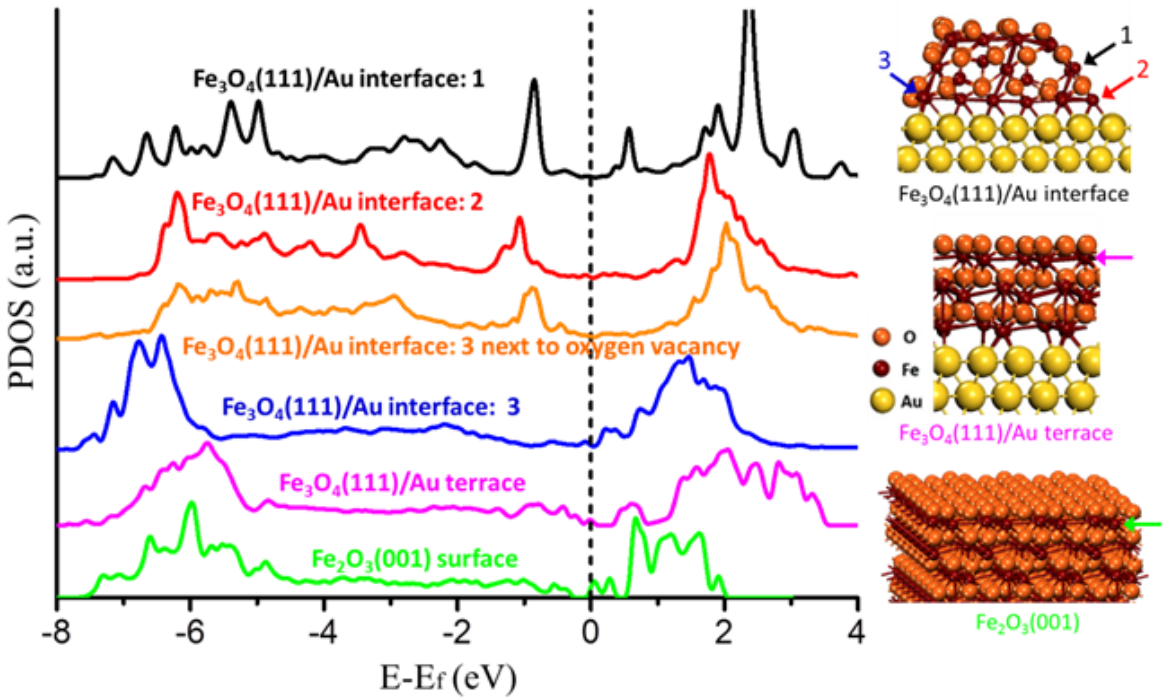

Figure 8. DFT-calculated partial density of states (PDOS) for Fe 3d on Fe_2O_3(001) surface, Fe_3O_4(111)/Au(111) terrace and Fe_3O_4/Au interface with and without oxygen vacancy. The position of Fe is labeled on the right panel.

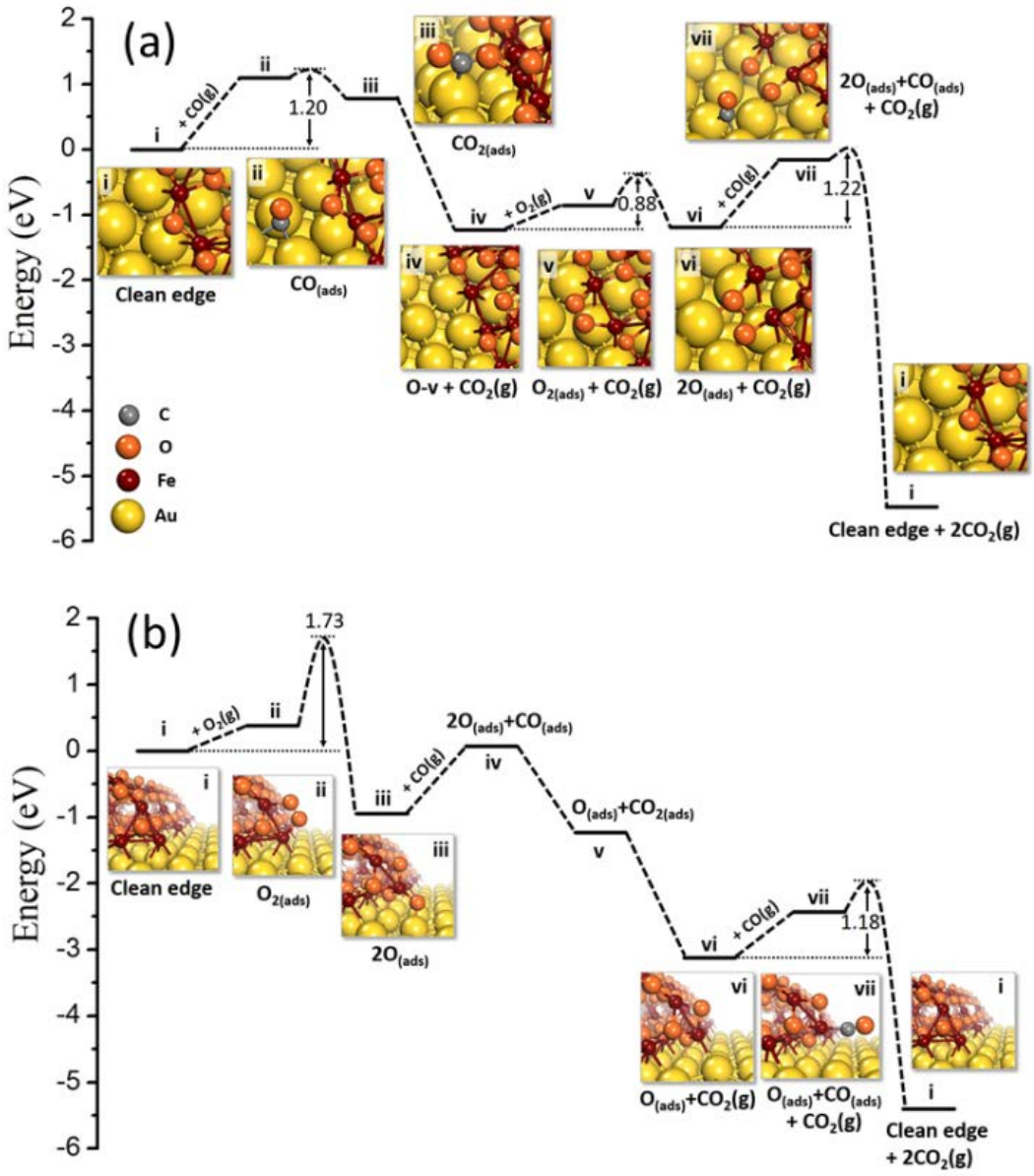

Figure 9. Potential energy diagram and corresponding reaction intermediates for CO oxidation at the interfacial sites of (a) $Fe_3O_4(111)/Au(111)$ interface and (b) $Fe_3O_4(100)/Au(111)$ interface. The entropy contributions at 575K for the steps involving gas phase CO, O_2 and CO_2 were included.
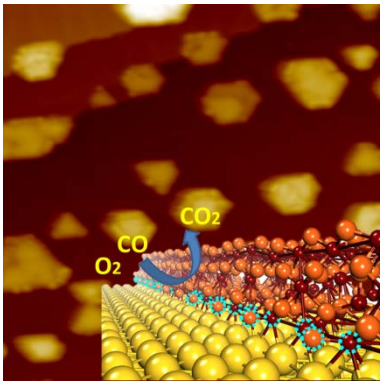
Table of Contents